REPORT DOCUMENTATION PAGE

Form Approved
OMB No. 0704-0188

1. AGENCY USE ONLY (Leave blank)	2. REPORT DATE	3. REPORT TYPE AND DATES COVERED
	10 October 1994	Technical 6/1/94–5/31/95

4. TITLE AND SUBTITLE
Small Cavity Nonresonant Tunable Microwave–Frequency Alternating Current Scanning Tunneling Microscope

5. FUNDING NUMBERS
N00014-91-J-1630

6. AUTHOR(S)
L. A. Bumm and P. S. Weiss

7. PERFORMING ORGANIZATION NAME(S) AND ADDRESS(ES)
Department of Chemistry
152 Davey Laboratory
The Pennsylvania State University
University Park, PA 16802

8. PERFORMING ORGANIZATION REPORT NUMBER
Report #21

9. SPONSORING / MONITORING AGENCY NAME(S) AND ADDRESS(ES)
Office of Naval Research
Chemistry Program
800 N. Quincy Street
Alexandria, VA 22217–5000

10. SPONSORING / MONITORING AGENCY REPORT NUMBER

11. SUPPLEMENTARY NOTES
Prepared for publication in *Review of Scientific Instruments*

12a. DISTRIBUTION / AVAILABILITY STATEMENT
Approved for public release.
Distribution unlimited.

12b. DISTRIBUTION CODE

13. ABSTRACT *(Maximum 200 words)*

We have developed a broadly tunable microwave frequency alternating current scanning tunneling microscope which employs a cavity with no resonances in the frequency range used. This results in a low flat background for spectroscopic measurements with this instrument.

14. SUBJECT TERMS	15. NUMBER OF PAGES
	20 pages
	16 PRICE CODE

17. SECURITY CLASSIFICATION OF REPORT	18. SECURITY CLASSIFICATION OF THIS PAGE	19. SECURITY CLASSIFICATION OF ABSTRACT	20. LIMITATION OF ABSTRACT
Unclassified	Unclassified	Unclassified	UL

Small Cavity Nonresonant Tunable Microwave–Frequency Alternating Current Scanning Tunneling Microscope

L. A. Bumm and P. S. Weiss*
Department of Chemistry
The Pennsylvania State University
University Park, PA 16802–6300
USA

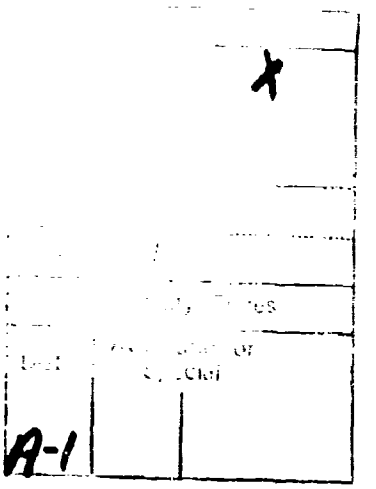

Abstract

We have developed a broadly tunable microwave frequency alternating current scanning tunneling microscope which employs a cavity with no resonances in the frequency range used. This results in a low flat background for spectroscopic measurements with this instrument.

*Author to whom correspondence should be addressed.

I. INTRODUCTION

The alternating current scanning tunneling microscope (ACSTM) extends the capabilities of the STM from a simple atomic scale topographic and local density of states (LDOS) probe to a spectroscopic probe capable of measuring local variations in chemical, dielectric, and magnetic properties.[1-10] Spectroscopic contrast has already been observed on several surfaces,[5,6] but its interpretation is not resolved. In addition, the ACSTM extends the capabilities of the tunneling microscope beyond conducting substrates to enable imaging and local spectroscopy on insulators.[1-10]

Kochanski first demonstrated ACSTM operation on insulators and semiconductors by detecting the third harmonic of the applied bias frequency in a cavity resonant at the detection frequency.[1] This scheme has since been applied by others to study substrates ranging from metals to insulators[2,3] and to measure doping profiles in silicon.[6] In our previous work, we have avoided the use of a resonant cavity in favor of retaining broadband frequency response.[4,7-10]

The ACSTM is conceptually very similar to conventional STM. The sample is scanned by a piezoelectrically driven probe tip controlled by a feedback signal sensitive to the probe tip–sample gap distance. In ACSTM a high (typically microwave) frequency bias is applied to the probe tip. We can apply a bias at any frequency from DC to 20 GHz,[11] an additional variable with which to interrogate the surface under study. The response that can be expected varies from quasi–static at low frequencies to dispersive at high frequencies. In the quasi–static limit the ACSTM can be treated as a conventional STM experiment with a time–varying DC bias. In this limit there is no extra information in the bias frequency domain.[12] At sufficiently high frequencies, the tunnel junction response becomes dispersive. This deviation from quasi–static behavior is due to the inability of the system to follow the rapidly oscillating AC field. By mapping the frequency and amplitude

dependence of this response, we can determine the origin(s) of these effects and use this information to elucidate the local chemical, electronic, and/or structural properties of the substrate surface.[8,10]

Only a small fraction of the power incident on the ACSTM probe tip is expected to interact with the tunneling junction.[13] Therefore the response signal due to the tunneling junction will be small compared to the total incident power at the fundamental frequency. Further complications arise from non–local interactions of the probe with its surroundings which can dominate the ACSTM response at the fundamental frequency. These non–local interactions can affect the microwave energy in the tunneling junction, thus complicating the interpretation of the local non–linear signal as well. Minimizing the non–local interactions is desirable for any ACSTM detection scheme and is the focus of this report.

II. INSTRUMENT DESIGN

The microwave signal from the ACSTM is sensitive not only to the properties of the tunneling junction, but also to electromagnetic interactions with structures within and surrounding the ACSTM. At microwave frequencies these interactions can dominate the AC response if not properly considered in the design. We have found two interactions to be critical: 1) radiation from the probe tip coupling to cavity modes of the ACSTM electromagnetic interference (EMI) and acoustic shield enclosure, and 2) reflections within the coaxial cable to the probe tip leading to standing waves in this line. The ACSTM design described herein operates in air and minimizes these effects.

A. Cavity Modes

The ACSTM is enclosed in an aluminum cylinder which serves to isolate the ACSTM from its surroundings electromagnetically and acoustically. Unfortunately, the EMI and acoustic shield and its contents also act as an electromagnetic resonant cavity to which the ACSTM probe tip can radiatively couple. For this cylindrical cavity with a height of 24.5 cm and a diameter of 19.6 cm (neglecting the enclosed structures: the STM, the vibration isolation viton stack, the lead wires,

etc.), the lowest frequency resonant mode is the TE_{111} at 1.09 GHz.[14] This mode defines the cutoff frequency of the cavity, below which all modes are evanescent. Since these modes generally do not have TEM character, the field structures of the high order modes become spatially complex. The nature of the coupling of the tip to these modes, *e.g.* resonant or antiresonant, is thus complex and depends not only on the frequency but also on the position of the probe tip and the sample probe within the mode field pattern and the radiation characteristics of the probe tip. Coupling between the probe tip and the sample probe can also be mediated by the cavity modes. Additionally, the high Q of cavity resonators, *ca.* 10^4,[15] will give rise to very sharp features in the probe tip–sample probe coupling.

Cavity modes can be suppressed by introducing absorbers into the cavity to lower the Q of these modes. At these frequencies absorbers are typically either ferromagnetic resonant or resistive. We have fabricated microscope parts from a ferromagnetic resonant absorber material, Ferrosorb (for an example, see the sample elevator in Fig. 4 of Ref. 7).[16] This is effective at high frequencies where the iron particles ferromagnetically resonate and the probe tip radiation is most significant. Effective over a broader frequency range is the introduction of ohmic losses at the enclosure walls by lining them with carbon–loaded conductive foam,[18] the type used for storing electronic devices. Combined, these absorbers have a dramatic effect in reducing these cavity modes (see Fig. 1).[19] Note that the effects of standing waves remain and can be observed in trace B of Fig. 1.

If the enclosure could be made small enough so that the highest frequency of interest, 22 GHz,[20] was below the cut–off frequency of the cavity, the system would be completely free of cavity mode interferences. For a similarly proportioned cylinder, a diameter less than 1 cm would be required. Fortunately only the tip–sample region need be enclosed by the cavity not the entire ACSTM, and consequently an enclosing cavity was created within the ACSTM structure. This was realized as a two–part cavity which did not compromise the function of the beetle–style STM[7,21] as shown in

Fig. 2. The sample holder serves as the upper part of the cavity (C) and includes the beetle walker ramps (D). The lower part of the cavity (E) contains the ACSTM probe tip (A) and is mounted on the scanner piezoelectric tube (G). Electrical contact between the two parts is achieved by means of a liquid metal seal,[22] which has the advantage that it allows unhindered rotation and translation of the sample holder as required for tip–sample approach in the beetle-style STM. The liquid metal (F) is held in a circular trough in the lower portion of the cavity (E). A short segment of stainless steel tubing (I), is soldered to the upper portion of the cavity (C) and protrudes down into the trough of liquid metal forming a continuous electrical contact. A complication of this small cavity design is that the sample (B) is at the same potential as the shielding enclosure (C, E, and I). This can be overcome by applying a DC bias to the transimpedance (low frequency) amplifier. Alternatively we have also applied a DC bias to the sample via a small battery (L) in Fig. 2. In this case the sample is mounted on one terminal of the battery and the other is connected to the sample holder (M). Hence the small cavity ACSTM can be operated simultaneously or independently as a conventional STM.

B. Standing Waves

Standing waves result from the interference of one or more waves, which here consist of the incident wave from the microwave source and the waves reflected at transmission line discontinuities. The most important "discontinuity" is the ACSTM tunneling junction itself which behaves like an open circuit termination, reflecting nearly all the incident energy. If there were no other reflections, the reflected power vs. frequency would depend only on the changing environment of the ACSTM probe tip. If there are other reflections due to interfaces within the transmission lines, these will interfere with the wave reflecting from the tunneling junction, resulting in periodic constructive and destructive interferences in the frequency domain as shown in Fig. 3.[23] These reflections not only cause interferences in the reflected wave, but also in the wave incident on the ACSTM probe tip via

multiple reflections. These interferences also affect the detection leg of the instrument leading to variations in instrument sensitivity with detection frequency.

The effects of standing waves in the ACSTM probe tip design of Ref. 4 can readily be seen by measuring S_{11} vs. frequency[24] for the probe tip as shown in trace A of Fig. 3. The two large peaks are caused by a transmission line discontinuity due to the 14 mm of the coaxial transmission line closest to the ACSTM probe tip, constructed from stainless steel hypodermic syringe tubing and PTFE tubing (see Fig. 2 of Ref. 4). The dimensions had been chosen for convenience of construction and resulted in a characteristic impedance of 13 Ω for this section. When optimally coupled to the 50 Ω UT34 semi-rigid coaxial line[25] that leads away from the ACSTM, the impedance mismatch yields a reflection coefficient of 34% for this interface.[26] The smaller amplitude variations in trace A of Fig. 3 are caused by an impedance discontinuity at the UT34–SMA[27] connection to the source cable, with an estimated reflection coefficient of 10%. Two features are common to both traces A and B of Fig. 3. The reflected power decreases with increasing frequency due to attenuation in the coaxial cable. This causes a correlated increase in the amplitude of the interference pattern resulting from the increase in the proportion of reflected power from the SMA connector. Over all, the structure in the microwave signals from the ACSTM probe tip has been greatly reduced by properly impedance matching and terminating the microwave transmission lines.

The 13 Ω coaxial cable (used in Refs. 4) was replaced by a segment of UT70-LL semi-rigid coaxial cable[25] which has a 50 Ω characteristic impedance and still meets the dimensional requirements. Namely the outer diameter 0.070" is small enough to fit inside our piezoelectric tube scanner, and the center conductor (0.020" diameter) is the same diameter as a standard hypodermic syringe tube.[28] Substitution of the syringe tube for the center conductor forms a coaxial transmission line with a hollow center conductor (0.012" inner diameter) which can capture the tip in precisely the same manner as in our earlier design. Specifically the 0.010" diameter shaft of the controlled

geometry Pt–Ir tips[29] are kinked slightly, forming a spring which holds them in place once inserted into the syringe tube center conductor. This forms the 50 Ω coaxial transmission line leading to the ACSTM probe tip.

Smaller diameter semi–rigid coaxial cable (UT34) connects the UT70–LL probe tip section and the microwave test equipment. The mechanical flexibility of this cable gives better vibration isolation and convenience than larger diameter semi–rigid cables. The resulting transition between coaxial cables of different sizes must be carefully designed since it can seriously impact the microwave performance of the system even though both transmission lines have the same characteristic impedance. The standard procedure is to create a compensation step, *viz.* a small offset between the planes of the steps in the outer and inner diameters at the junction (see Fig. 4).[30] The resulting S_{11} in trace B of Fig. 3 shows that the standing waves have been largely eliminated. The remaining oscillations are due to one poorly compensated transition in the SMA connector[27] at the test equipment end of the UT34 microwave coaxial cable.

C. Transmission Line Termination

Cavity mode interference can be further reduced by decreasing the radiation from the probe tip. This is achieved by establishing a well–defined plane of termination of the coaxial transmission line. In our earlier design (see Fig. 2 of Ref. 4) the center conductor of the coaxial line simply protruded 0.050" beyond the end of the shield. This left the electrical length of the ACSTM tip ill–defined, since this length depends not only on the distance that the center conductor extends beyond the shield, but also on the length and geometry of the shield. The ground plane in the small cavity ACSTM is defined by the lower half of the small cavity as described above and shown in Fig. 2. If the radial extent of the ground plane is larger than the distance that the tip extends above it, there is an effective reference plane for defining the electrical length of the probe tip.[32] The flat region (F) in the center of Fig. 2 has an inner radius of 0.1" which is twice the extension of the probe tip

above the plane and has an outer radius is 0.2". This structure roughly approximates a short vertical monopole (a dipole if the center conductor and its image charge are considered), which resonates when its length is one–quarter of the wavelength of the applied microwave radiation ($\lambda/4$). For a probe tip extension, $l = 0.05$", this occurs at 59 GHz. For $l \leq \lambda/4$, the radiation from the antenna is proportional to l^6/λ^4.[33] Hence the combination of a short probe tip extension and a well–defined ground plane efficiently reduces probe tip radiation.

III. ASSEMBLY AND OPERATION

Due to the limited vertical range of the walker ramps for the coarse approach, the tip and sample separation must be adjusted prior to tunneling. Controlled geometry Pt–Ir tips[29] are used in the ACSTM (A in Fig. 2). The protrusion of these tips from the ground plane (F in Fig. 2) is adjusted. Silver paint[34] is used to mount and to make electrical contact to the samples.

It is particularly important in the small cavity ACSTM design to limit the lateral motion during coarse approach, since a misalignment of the two halves of the cavity of 0.050" results in contact and hinders further motion. This is achieved by modification of the walker ramps. Helical grooves were milled into the ramps using a 1/8" hemispherical end mill with a pitch of 0.040" in 120°.[35] Since the 1/8" diameter groove rests on 1/16" ball bearings, enough lateral motion is retained to survey the surface by walking the sample holder sideways using the outer walker piezoelectric tubes.[21]

The liquid metal seal also requires special attention. The In/Ga/Sn liquid metal alloy does not wet the titanium trough. Due to the small dimensions of the channel in the lower half of the cavity, it tends to bead up under surface tension. With care, the alloy is made to wet the stainless steel walls of the small cavity sufficiently to ensure continuous electrical contact so long as enough liquid metal is placed in the channel. The cavity is assembled by attaching the top part of the cavity (C or M in Fig. 2) into the coarse approach ramps (D in Fig. 2), then loading the ramps into the elevator to be

lowered onto the STM. Continuity of the liquid metal seal is verified by measuring the resistance between the top and bottom halves of the cavity.[36] From this point on the operation of the ACSTM is identical to that described in Ref. 7.

We demonstrate the operation of this ACSTM with images of an amorphous region of a gold film evaporated on mica as shown in Fig. 5. The experiment was performed in air under DC feedback control using the internally biased sample holder described above (with V_{tip}=1.4V and I_{tunnel}=100 pA). A microwave bias at 18.3775 GHz (+10 dBm) was simultaneously applied to the tip. The microwave energy reflected from our sample at the modulation frequency was measured using the spectrum analyzer (through a directional coupler).[20] The microwave frequency reflected signal is highly correlated with the simultaneously recorded topography.

IV. CONCLUSIONS AND FUTURE PROSPECTS

Implementation of these improvements has greatly reduced the frequency domain artifacts caused by interactions other than at the tunnel junction. Hence frequency domain measurements can now be made without the need to compensate for cavity mode and standing wave resonant effects, thus improving the signal–to–noise ratio. This broadband ACSTM design terminates the coaxial shield in a ground plane and keeps the distance that the probe tip extends above that plane as short as possible. We have found that electromagnetic interactions unrelated to the tunnel junction properties can dominate the AC response of the ACSTM. These interactions, specifically 1) cavity modes, 2) standing waves, and 3) radiation, must be systematically eliminated or minimized in any ACSTM design. These were addressed here by 1) forming a small nonresonant cavity and applying microwave absorbers, 2) careful attention to impedance matching and compensating transitions, and 3) properly terminating the ACSTM probe tip, respectively.

Acknowledgments

The authors would like to thank Rick Baer, Steve Clark, Dave Critelli, Samuel Condo, Stephan Stranick, Barry Willis, and Michael Yoshikawa Youngquist for assistance in the design and fabrication of this instrument. The support of the Biotechnology Research and Development Corporation, Hewlett–Packard, the National Science Foundation, and the Office of Naval Research are gratefully acknowledged.

REFERENCES

1. G. P. Kochanski, *Phys. Rev. Lett.* **62**, 2285 (1989).
2. B. Michel, W. Mizutani, R. Schierle, A. Jarosch, W. Knop, H. Benedikter, W. Bachtold and H. Rohrer, *Rev. Sci. Instrum.* **63**, 4080 (1992).
3. W. Seifert, E. Gerner, M. Stachel and K. Dransfeld, *Ultramicroscopy* **42–44**, 379 (1992).
4. S. J. Stranick and P. S. Weiss, *Rev. Sci. Instrum.* **64**, 1232 (1993).
5. S. J. Stranick, P. S. Weiss, A. N. Parikh, and D. L. Allara, *J. Vac. Sci. Tech. A.* **11**, 739 (1993).
6. J.–P. Bourgoin, M. B. Johnson and B. Michel, *Appl. Phys. Lett.* (1994), in press.
7. S. J. Stranick and P. S. Weiss, *Rev. Sci. Instrum.* **65**, 918 (1994).
8. S. J. Stranick and P. S. Weiss, *J. Phys. Chem.* **98**, 1762 (1994).
9. S. J. Stranick, M. M. Kamna, and P. S. Weiss, *Rev. Sci. Instrum.* **65**, 3211 (1994).
10. S. J. Stranick, L. A. Bumm, M. M. Kamna, and P. S. Weiss, in *Photons and Local Probes*, O. Marti and R. Möller, eds., *NATO ASI Series E: Applied Sciences* (Kluwer Academic, 1995).
11. The bias frequency range 0–20 GHz is limited only by the sources. The microwave frequency source, a Hewlett–Packard 83620A has a range of 10 MHz to 20 GHz. Lower frequencies, DC–30 MHz are supplied by a Hewlett–Packard 3314B function generator. Hewlett–Packard, Palo Alto, CA.
12. In the quasi–static small amplitude limit, detection of bias frequency harmonics can be used to measure the corresponding derivatives of the I–V characteristic at the DC bias point.
13. L. A. Bumm and P. S. Weiss, unpublished results. In the current geometry parasitic shunt capacitance plays a major role in limiting the microwave power that couples to the tunnel junction.
14. S. Ramo, J. R. Whinnery, and T. Van Duzer, *Fields and Waves in Communication Electronics*, 2nd ed. (John Wiley, New York, 1984).
15. L. W. Couch, II, *Digital and Analog Communication Systems*, 3rd ed. (Macmillan, New York, 1990).

16. Ferrosorb is an epoxy loaded with finely divided iron ("carbonyl iron" prepared by decomposition of $Fe(CO)_5$),[17] Ferrosorb Department, Microwave Filter Co., Inc., 6743 Kinne St., East Syracuse, NY 13057.

17. K. H. Roll, "Powder Metallurgy," in *Kirk–Othmer Encyclopedia of Chemical Technology,* 3rd ed., Vol. 19 (John Wiley, New York, 1982), p. 28.

18. Desco Industries, high density foam part #A12650, 1" thick, 761 Penarth Ave., Walnut, CA 91789.

19. These S_{21} (transmission) traces are sampled at 25 MHz intervals with an inherent bandwidth of less that 10 Hz, so that many high Q modes may not be observed.

20. The upper frequency limit of our spectrum analyzer is 22 GHz (Hewlett–Packard 71210C).

21. K. Besocke, *Surf. Sci.* **181**, 145 (1987); J. Frohn, J. F. Wolf, K. Besocke, and M. Teske, *Rev. Sci. Instrum.* **60**, 1200 (1989).

22. The liquid metal we use is a gallium–indium–tin eutectic, Ga:In:Sn; 62:25:13, ÆSAR, Johnson–Matthey, 30 Bond St., P.O. Box 8247, Ward Hill, MA 01835–0747.

23. Only these interferences are observed directly,

24. The term S_{ji} is a scattering parameter[14] which is the ratio of the signal measured at port j to that applied at port i. S_{ji} is a complex quantity with both magnitude and phase components. We use the term, S_{ji}, loosely in the text to mean the magnitude, $|S_{ji}|$. Hence S_{11} represents that ratio of reflected to incident power (the power reflection coefficient), while S_{21} is the ratio of the transmitted to the incident power (the power transmission coefficient).

25. Micro–Coax Components, Inc., West 5th Ave., Box E, Collegeville, PA 19426.

26. In this article we refer always to the *power* reflection coefficient.

27. Huber & Suhner, Inc., Model #11 SMA–50–1–1c, 500 West Cummings Park, Suite 2000, Woburn, MA 01801.

28. Small Parts, Inc., 13980 N.W. 58th Court, P. O. Box 4650, Miami Lakes, FL 33014–0650.

29. Materials Analytical Services, 2418 Blue Ridge Rd., Suite 105, Raleigh, NC 27607.

30. The need for this compensation step can be understood via the lumped circuit model.[31] When the planes of the two steps coincide, the fringing capacitance between the shoulders of the outer

and inner diameter steps create a region of low impedance at the transition (a shunt capacitance). Offsetting the planes of the steps slightly to create a third region of high impedance adds a series inductance which then compensates for the fringing capacitance. Without this compensation the fringing capacitance will cause a reflection from the transition region.

31. J. R. Whinnery and H. W. Jamieson, *Proc. IRE*, **32**, 98 (1944); J. R. Whinnery, H. W. Jamieson and T. E. Robbins, *Proc. IRE*, **32**, 695 (1944); N. Marcuvitz, ed., *Waveguide Handbook* (McGraw–Hill, New York, 1951); T. S. Saad, ed., *Microwave Engineer's Handbook*, Vol. 1, (Artech House, Dedham, 1971); K. C. Gupta, "Transmission–Line Discontinuities," in *Handbook of Microwave and Optical Components*, Vol. 1, K. Chang, ed. (John Wiley, New York, 1989), pp. 60–117.

32. *The ARRL Handbook for Radio Amateurs*, 70th ed. (The American Radio Relay League, Newington, 1993).

33. E. C. Jordan, *Electromagnetic Waves and Radiating Systems* (Prentice–Hall, New York, 1950).

34. Pelco Colloidal Silver, Ted Pella, Inc., P.O. Box 492477, Redding, CA 96049–2477.

35. This approach was first taken by M. G. Yoshikawa Youngquist, J. H. Ferris, and P. S. Weiss. It has the additional advantage that the coarse approach centers the STM probe tip on small samples.

36. We note that due to the well–defined ground plane (see Sec. II.C) the ACSTM works nearly as well even with incomplete electromagnetic enclosure. We will use this configuration in ultrahigh vacuum where full enclosure by a liquid metal seal would not be possible.

FIGURE CAPTIONS

Fig. 1. Electromagnetic cavity modes of the EMI/acoustic shield are detected by the coupling between the ACSTM probe tip and sample. S_{21} (transmission) vs. frequency is measured. The probe tip design is that of Ref. 7.

A) The cavity modes manifest themselves as the structure in S_{21}.

B) This curve has been offset by +40dB for clarity. The conditions are identical to A, except that the microwave absorbers described in the text were introduced into the cavity.

Fig. 2. Cross–section of the tip–sample region showing the small cavity ACSTM with the liquid metal seal and optional internally biased sample holder (above).

A) tip, B) sample, C) top of the cavity and sample holder (copper), D) beetle ramps (titanium), E) lower part of the cavity (titanium), F) liquid metal, G) piezoelectric scanner tube, H) UT70–LL ACSTM probe tip assembly, I) stainless steel tubing contacting the liquid metal, J) macor spacer, K) piezoelectric beetle walker tubes, and optional: L) battery forming the top of the cavity, and M) battery mount. The assembly forming the top part of the cavity is held in pace by spring clips formed from beryllium copper (not shown).

Fig. 3. A comparison of S_{11} (reflected signal) vs. frequency for two ACSTM designs.

A) S_{11} for the ACSTM design described in Ref. 7. The large features at 7.5 and 15 GHz are due to destructive interference from reflections at the probe tip and the 50 Ω – 13 Ω interface. The smaller features are caused by interference of the ACSTM probe tip and the SMA connector reflections. A second periodicity is due to the interference of the waves reflected at the 50 Ω – 13 Ω transition and at the SMA connector.

B) S_{11} for the small cavity nonresonant ACSTM design. The curve has been offset by +10dB for clarity. The remaining structure is caused by the SMA connector shunt capacitance.

Fig. 4. Diagram of the compensating transition between the UT70-LL and the UT34 semi-rigid semi-rigid coaxial cables. The center conductor of the UT70-LL has been replaced by stainless steel hypodermic syringe tube (0.020" outer diameter and 0.012" inside diameter). Two bushings were used to form the transition. A first bushing assures concentricity of the center conductor junction and a second forms the connection between the shields.

Fig. 5. Simultaneously recorded conventional STM (A, left) and ACSTM (B, right) images of a 500Åx500Å area of an amorphous region of a gold film evaporated on mica. The images were recorded under constant DC current feedback control with V_{tip}=1.4V and I_{tunnel}=100 pA using the internally biased sample holder. A microwave bias at 18.3775 GHz (+10 dBm) was simultaneously applied to the tip. The image on the right shows the microwave signal reflected from the ACSTM tip back to the spectrum analyzer (through a directional coupler) at the modulation frequency.

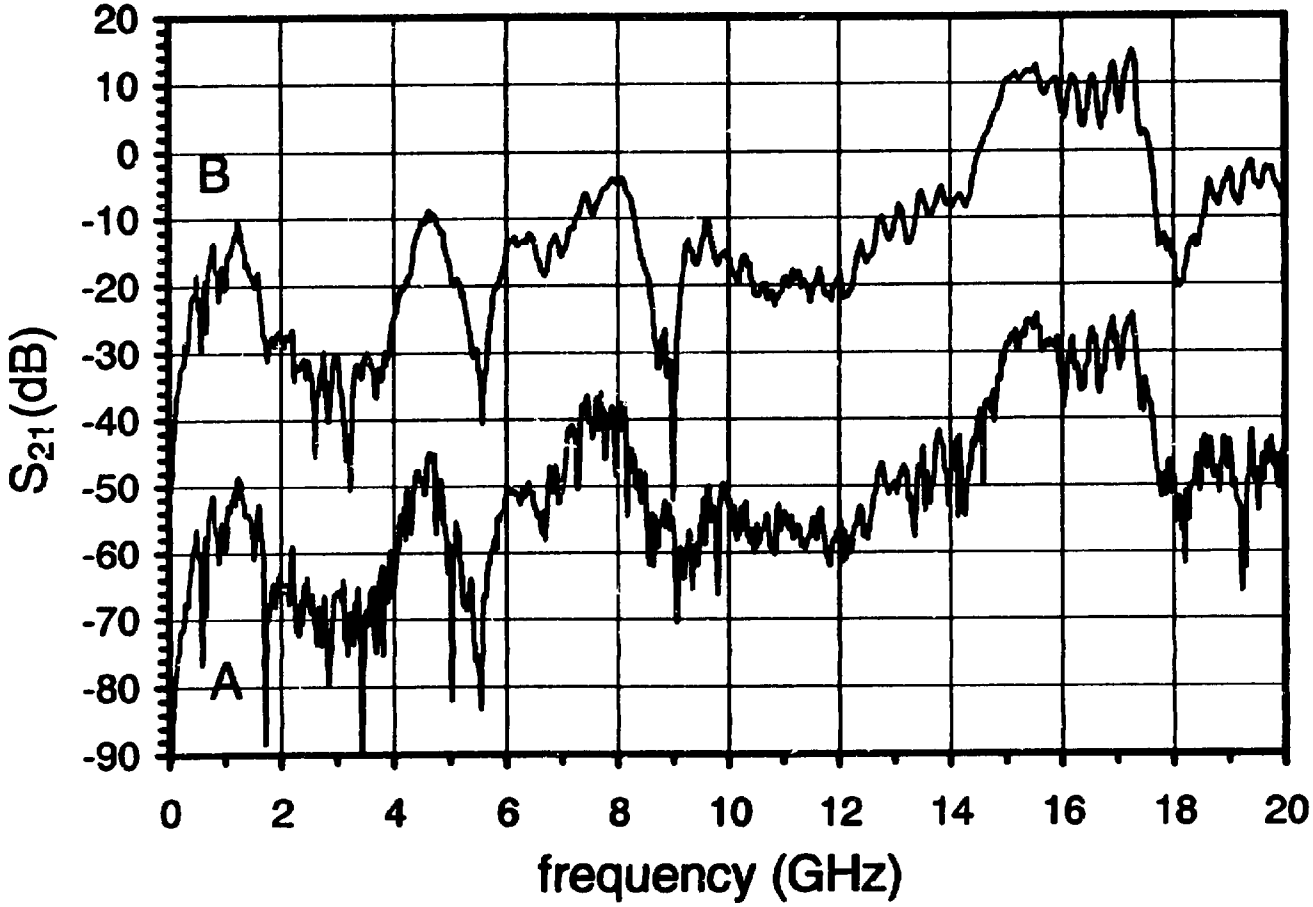
20
10
0
-10
-20
-30
-40
-50
-60
-70
-80
-90
B
A
S_{21} (dB)
0
2
4
6
8
10
12
14
16
18
20
frequency (GHz)

Fig. 1

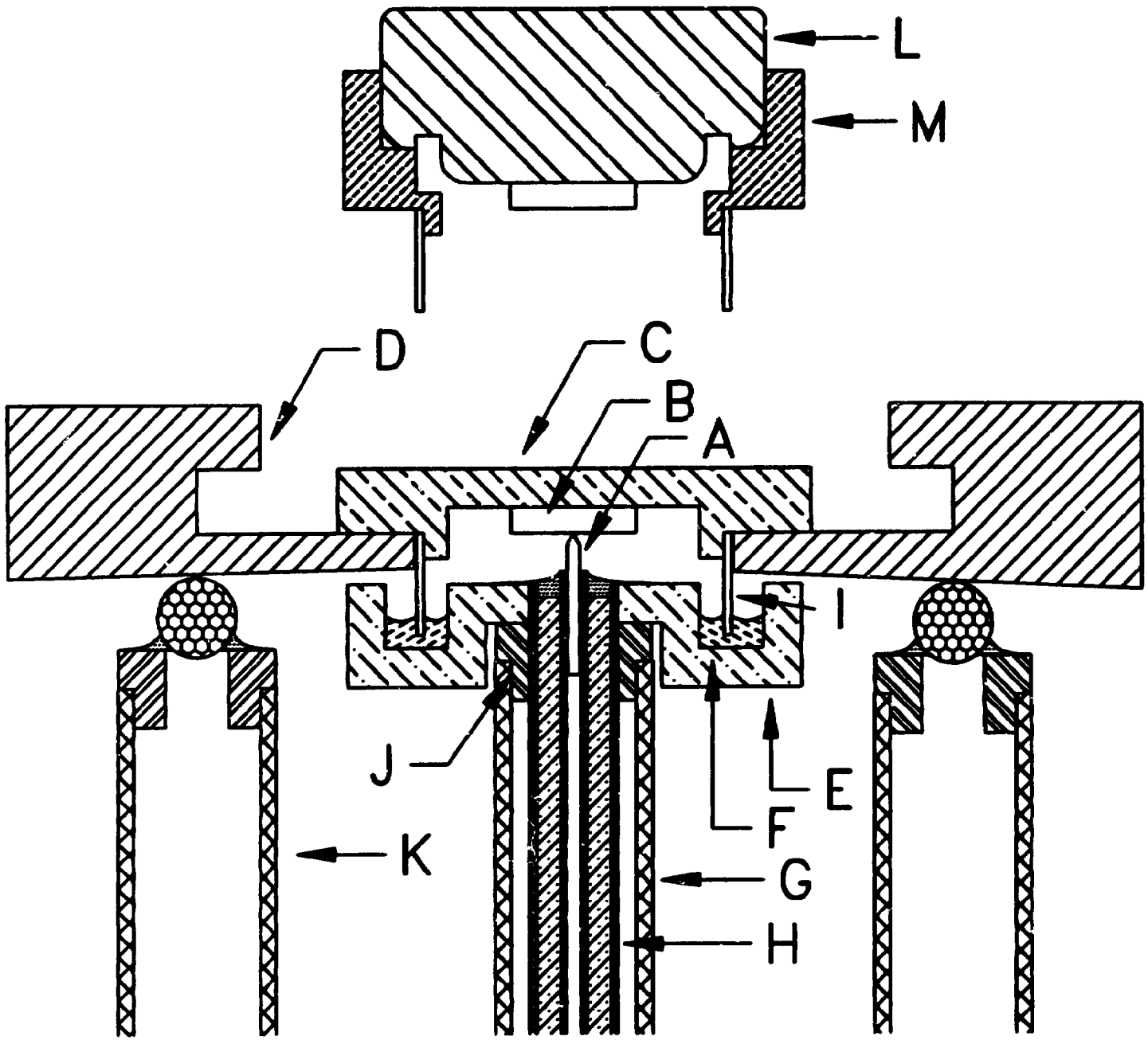

Fig. 2

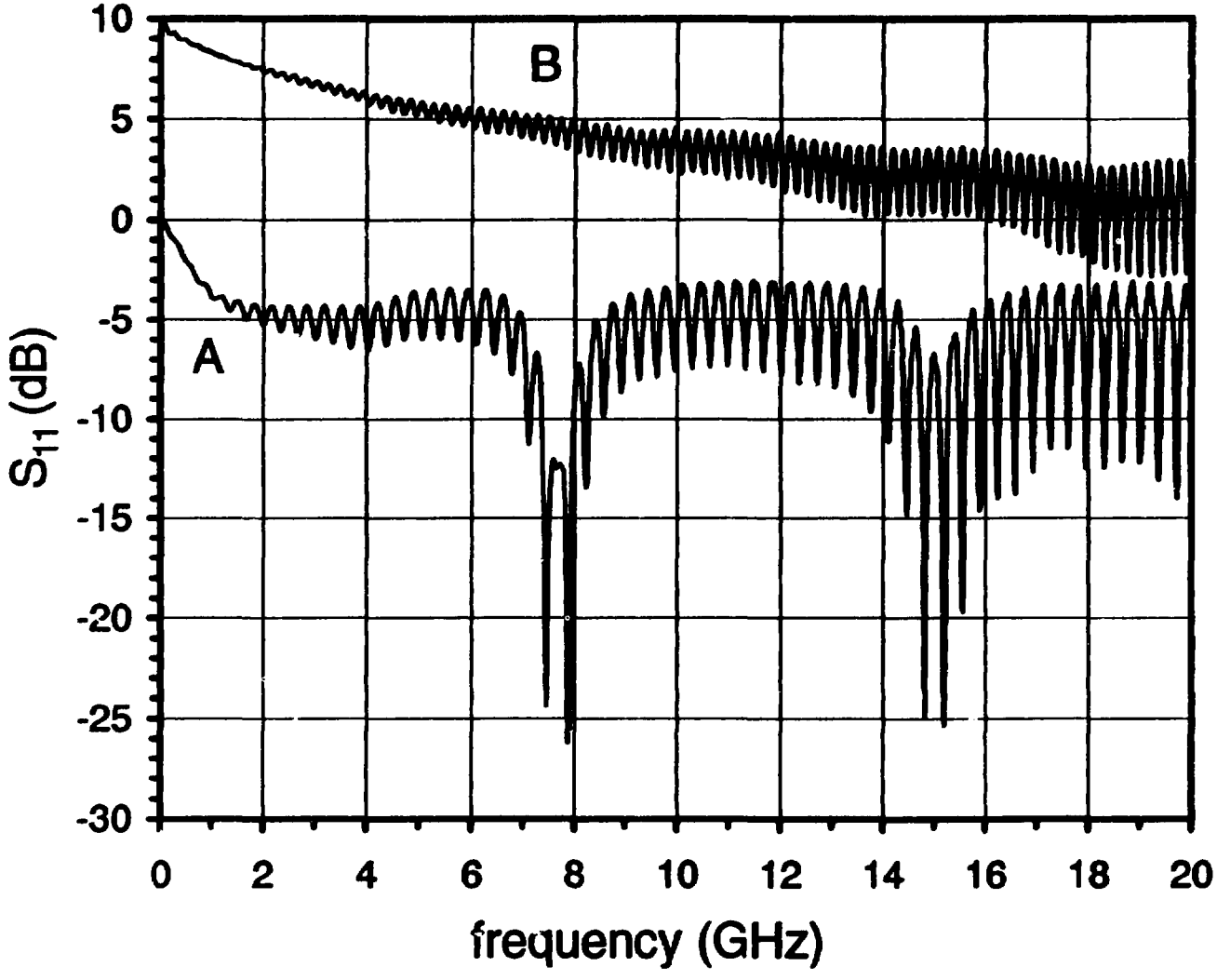
10
5
0
-5
-10
-15
-20
-25
-30
B
A
S_{11} (dB)
0
2
4
6
8
10
12
14
16
18
20
frequency (GHz)

Fig. 3

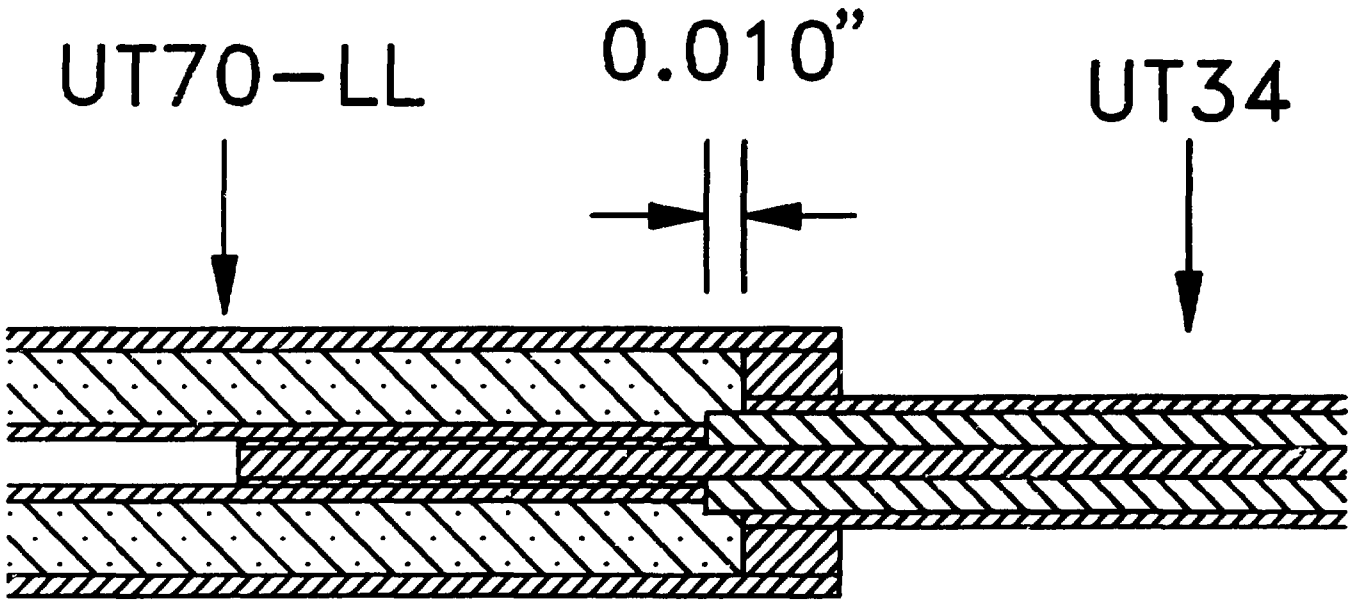

Fig. 4

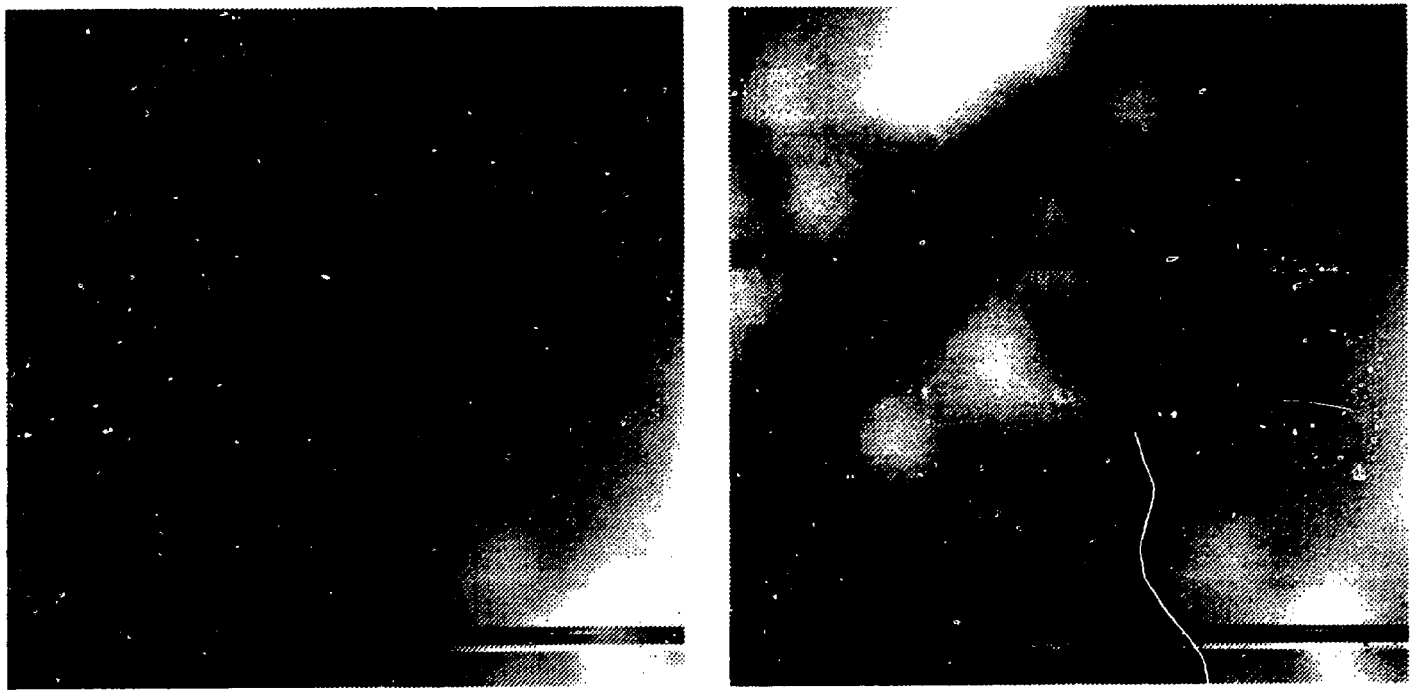

A B

Fig. 5